As per UGC guidelines an electronic bar code is provided to secure your paper

International Journal for Modern Trends in Science and Technology
Volume 11, Issue 06, pages 25-38.
ISSN: 2455-3778 online
Available online at: http://www.ijmtst.com/vol11issue06.html
DOI: https://doi.org/10.5281/zenodo.15576830

Coordinated Control and Power Quality Enhancement of a Hybrid DC/AC Microgrid Using DPFC and Renewable Energy Integration

K. Vinod Kumar[1], K. Venkatapathi[2], Dr. K. Siva Kumar[3]

[1]PG Scholar, Dept. of Electrical & Electronics Engineering, Sri Venkatesa Perumal College of Engineering and Technology, Puttur, Andhra Pradesh, India
[2]Associate Professor, Dept. of Electrical & Electronics Engineering, Sri Venkatesa Perumal College of Engineering and Technology, Puttur, Andhra Pradesh, India
[3]Professor, Dept. of Electrical & Electronics Engineering, Sri Venkatesa Perumal College of Engineering and Technology, Puttur, Andhra Pradesh, India

To Cite this Article
K. Vinod Kumar, K. Venkatapathi & Dr. K. Siva Kumar (2025). Coordinated Control and Power Quality Enhancement of a Hybrid DC/AC Microgrid Using DPFC and Renewable Energy Integration. International Journal for Modern Trends in Science and Technology, 11(06), 25-38. https://doi.org/10.5281/zenodo.15576830

Article Info
Received: 13 May 2025; Accepted: 30 May 2025.; Published: 02 June 2025.

Copyright © The Authors ; This is an open access article distributed under the Creative Commons Attribution License, which permits unrestricted use, distribution, and reproduction in any medium, provided the original work is properly cited.

KEYWORDS

Hybrid DC/AC Microgrid, Distributed Power Flow Controller (DPFC), Photovoltaic (PV), Wind Turbine, Permanent Magnet Synchronous Generator (PMSG), Battery Energy Storage System (BESS), Power Quality, Total Harmonic Distortion (THD), Maximum Power Point Tracking (MPPT), Coordinated Control, DC Bus Voltage Regulation, Renewable Energy Integration.

ABSTRACT

This paper presents a coordinated control strategy for a hybrid DC AC microgrid integrating photovoltaic PV wind turbine driven permanent magnet synchronous generator PMSG and a battery energy storage system BESS focusing on improving power quality and system reliability using a Distributed Power Flow Controller DPFC. The system connects solar wind battery AC and DC loads including a PMSM based water pump to a common DC bus. AC linear and non-linear loads are connected between the DPFC and the DC microgrids to balance loads enable bidirectional power flow and ensure reliable supply to AC loads. A voltage source converter VSC at the grid side facilitates stable DC to AC power conversion. The DPFC comprising series and shunt converters compensates voltage disturbances such as sags and swells and mitigates current harmonics reducing Total Harmonic Distortion THD and improving voltage and current profiles. Maximum power extraction is achieved using MPPT algorithms for PV and wind systems while a bidirectional buck boost converter manages battery charge and discharge to balance demand and support transient events. A hierarchical control approach regulates DC bus voltage via the grid connected converter and stabilizes the system using the battery during grid disturbances. An energy management algorithm enables seamless transitions among DC voltage regulation power injection and hybrid operation. MATLAB Simulink simulations

of a 15.8 kW system demonstrate superior transient response reduced oscillations and enhanced power quality compared to conventional methods.

1. INTRODUCTION

The increasing global emphasis on sustainable energy solutions has driven the integration of renewable energy sources such as photovoltaic (PV) systems and wind turbines into modern power networks [1]. These renewable sources, characterized by their clean and inexhaustible nature, are vital for reducing greenhouse gas emissions and dependency on fossil fuels [2]. Hybrid DC AC microgrids have emerged as promising architectures for effectively integrating distributed energy resources (DERs), including PV panels, wind turbines, and energy storage systems, into local distribution networks [3]. Hybrid microgrids offer significant flexibility by supporting both AC and DC loads, which is advantageous given the increasing adoption of DC-powered devices and electric vehicles in residential, commercial, and industrial applications [4], [5]. The coexistence of diverse load types such as permanent magnet synchronous motors (PMSM) for water pumping and other DC and AC loads requires sophisticated power management to ensure system stability and efficiency [6], [7]. Despite these advantages, the intermittent and variable nature of renewable energy sources introduces significant challenges. Solar irradiance fluctuations and variable wind speeds cause power output variability, which, coupled with nonlinear loads, can induce voltage instability, power quality degradation, and increased harmonic distortion [8], [9]. These issues threaten the reliability of the microgrid and may lead to operational failures if not properly managed [10]. To mitigate these challenges, advanced control strategies are essential. Hierarchical control frameworks are commonly employed, with a primary control layer responsible for fast DC bus voltage regulation and immediate system response, while secondary control manages energy storage systems to stabilize the voltage and power sharing during sustained disturbances [11], [12]. Such control architectures enhance the microgrid's ability to maintain stable operation under varying load and generation conditions and support smooth transitions between grid-connected and islanded modes [13]. Power electronic converters such as voltage source converters (VSCs) play a pivotal role in interfacing renewable energy sources and loads with the DC bus and the utility grid. VSCs enable bidirectional power flow, seamless DC to AC conversion, and the integration of energy storage systems via bidirectional buck-boost converters to balance supply and demand [14], [15]. The efficient control of these converters is crucial to ensuring optimal power flow and maintaining power quality. One major concern in hybrid microgrids is the mitigation of power quality issues such as voltage sags, swells, and current harmonics caused by grid disturbances and nonlinear loads [16]. Traditional compensation techniques may not adequately address these issues in dynamic microgrid environments [17]. Distributed Power Flow Controllers (DPFCs), which combine series and shunt converters, have been proposed as advanced solutions to enhance power quality by compensating voltage disturbances and reducing Total Harmonic Distortion (THD) in current waveforms [18], [19]. The series converter in a DPFC primarily addresses voltage sags and swells by injecting appropriate voltage compensation signals, while the shunt converter mitigates current harmonics generated by nonlinear loads, thus improving the overall voltage and current quality in the microgrid [20]. The coordinated operation of these converters supports stable power exchange between the microgrid and the main grid and improves the system's robustness against disturbances [21]. To maximize the energy harvested from renewable sources, maximum power point tracking (MPPT) algorithms are implemented. For the PV system, perturb and observe (P&O) methods coupled with boost converters optimize power extraction under varying solar irradiance [22], [23]. Similarly, wind turbine systems employ VSC-based rectifiers with wind-speed-dependent MPPT controls to harness maximum energy from fluctuating wind speeds [24]. The integration of these MPPT techniques ensures the highest possible renewable power contribution to the microgrid. Energy storage systems, particularly batteries managed through bidirectional buck-boost converters, play a critical role in balancing the power demand and supply, as well as providing backup during transient disturbances or grid outages [25], [26]. Effective charge and discharge control of batteries helps maintain DC bus voltage stability and supports load requirements during intermittent renewable generation. Energy management algorithms coordinate the operation of all components in the microgrid, enabling smooth transitions between

different operating modes such as DC voltage regulation, power injection to the grid, and hybrid operation modes [27]. These algorithms optimize the microgrid's performance by prioritizing power flow according to system conditions and load demands. Simulation studies using platforms such as MATLAB/Simulink provide valuable insights into the transient behavior, stability, and power quality performance of hybrid DC AC microgrid systems with DPFC integration [28], [29]. These simulations have demonstrated that coordinated control strategies incorporating DPFCs significantly improve transient response times, reduce oscillations, and lower total harmonic distortion compared to conventional approaches [30].

2. System Configuration

The proposed hybrid DC/AC microgrid integrates photovoltaic (PV), wind, and battery energy storage sources into a common DC bus, enabling coordinated power sharing and stable operation. The PV array is connected through a boost converter that uses a perturb and observe (P&O) maximum power point tracking (MPPT) algorithm to ensure maximum power extraction under varying irradiance. A wind turbine drives a permanent magnet synchronous generator (PMSG), which produces variable-frequency AC power. This power is converted to DC using a voltage source converter (VSC) with wind-speed-dependent MPPT control. The DC output from both PV and wind systems feeds into the main DC bus. A bidirectional buck-boost converter is used to interface the battery energy storage system (BESS) with the DC bus. The converter manages battery charging and discharging based on load demand and renewable power availability. This helps in balancing power flow and maintaining DC bus voltage stability, especially during transient conditions or grid outages. The DC bus supplies both DC loads and an AC load through a voltage source converter (VSC) at the grid interface. A permanent magnet synchronous motor (PMSM)-based water pump is connected as a DC load, while linear and nonlinear AC loads are placed between the DC microgrid and the distributed power flow controller (DPFC). At the grid interface, the DPFC consists of both series and shunt converters. The series converter mitigates voltage disturbances such as sags and swells, while the shunt converter addresses current harmonic issues, thereby reducing total harmonic distortion (THD). Together, the DPFC improves power flow, voltage quality, and system stability. This configuration ensures reliable operation of the microgrid under diverse loading and environmental conditions, supporting bidirectional power flow and maintaining high-quality power delivery to all connected loads.

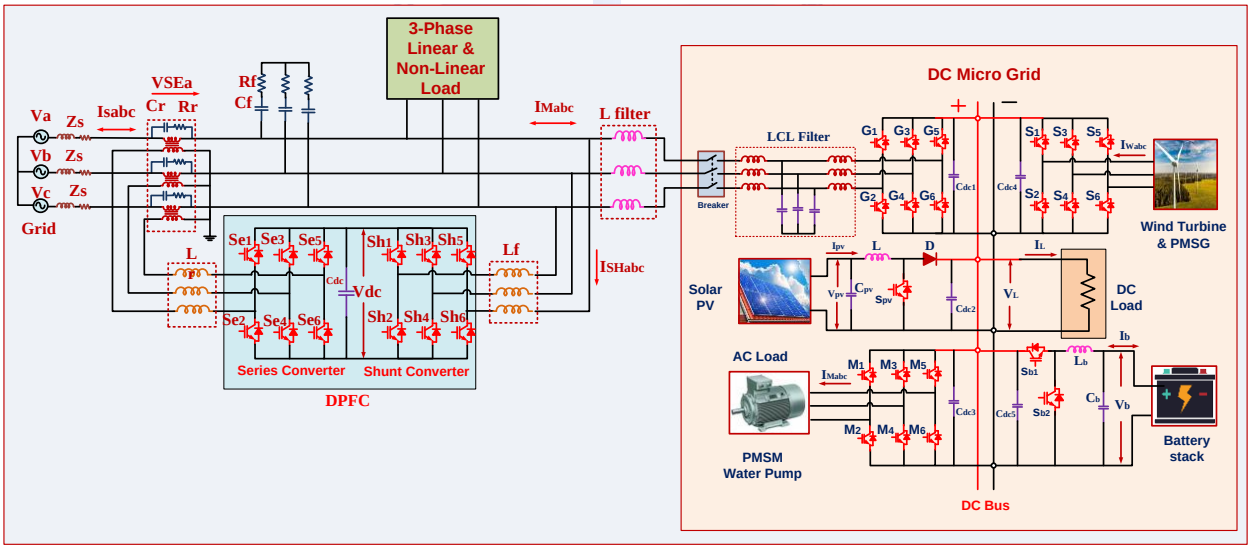

Fig.1 proposed system configuration

3. Modelling of DC/AC Microgrid

A. PV Cell Modeling

A photovoltaic array structured in series-parallel to attain the targeted voltage and current levels constitutes the solar configuration in the suggested hybrid microgrid. As seen in Figure 2, a DC-DC boost converter controls the output and ramps up the voltage before connecting the solar system to the DC bus. A Maximum

Power Point Tracking (MPPT) technique, usually utilizing the incremental conductance approach as illustrated in Fig.4, is used to optimize the energy captured from the solar panels under changing irradiance and temperature circumstances. In order to maintain a constant DC voltage on the bus, the converter works effectively to follow the maximum power point. Then, the DC output may be used for charging the energy storage system, powering DC loads directly, or even being reversed and fed to AC loads through the grid-connected converter. During daylight operation, the solar subsystem is essential for sustaining the microgrid's energy demands and ensuring the system's stability and sustainability.

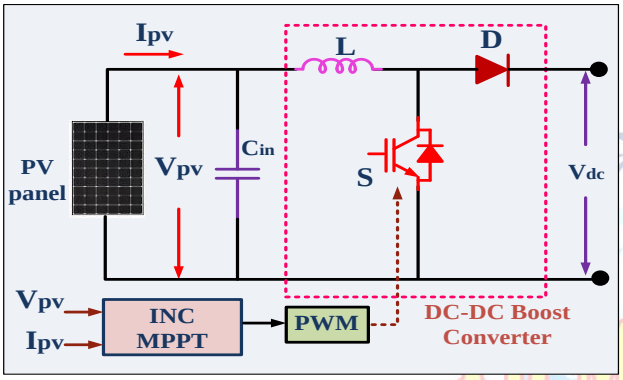

Fig. 2 solar PV INC MPPT DC-DC boost converter

For the solar photovoltaic (PV) system to be designed and modeled optimally, it is necessary to pick the right modules, set up the connections in series and parallel, and incorporate a DC-DC converter with maximum power point tracking (MPPT). Figure 3 shows the single-diode equivalent circuit that is used to describe each PV module. In this model, the output current is:

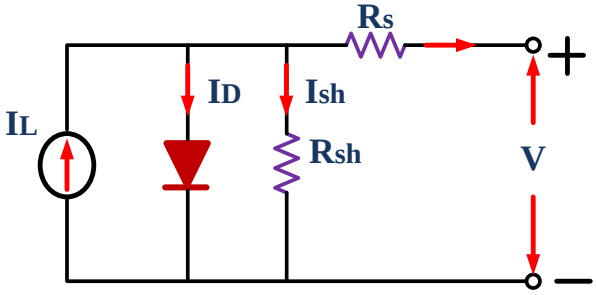

Fig. 3 equivalent model of PV solar.

$$I = I_{Ph} - I_0\left(e^{\frac{q(V+IR_S)}{nkT}} - 1\right) - \frac{V+IR_S}{R_{sh}} \qquad (1)$$

Here, I_{Ph} is the photocurrent, I_0 is the reverse saturation current, R_s and R_{sh} are the series and shunt resistances respectively, V is the terminal voltage, n is the ideality factor, T is the cell temperature in Kelvin, and q and K are the electronic charge and Boltzmann constant. The total power output is:

$$P_{PV} = V_{PV} \cdot I_{PV} \qquad (2)$$

To match the DC bus voltage, a boost converter is designed with the transfer function:

$$V_{out} = \frac{V_{in}}{1-D} \qquad (3)$$

Tracking the maximum power point involves modifying the duty cycle in response to variations in solar irradiance G and temperature T. The MPPT controller, which is usually an Incremental Conductance algorithm, is used for this purpose. When designing the converter, the parameters of the inductor L and capacitor C were chosen with Continuous Conduction Mode (CCM) in mind.

$$L = \frac{V_{in}\cdot(V_{out}-V_{in})}{\Delta I \cdot f_s \cdot V_{out}} \qquad (4)$$

$$C = \frac{I_{out}\cdot D}{\Delta V \cdot f_s} \qquad (5)$$

Where ΔI is the desired ripple in inductor current, ΔV is the ripple in output voltage, and f_s is the switching frequency. The output of the converter connects to the DC bus, supplying both DC loads and feeding into the grid through an inverter when needed. This model ensures optimal PV performance across varying environmental conditions.

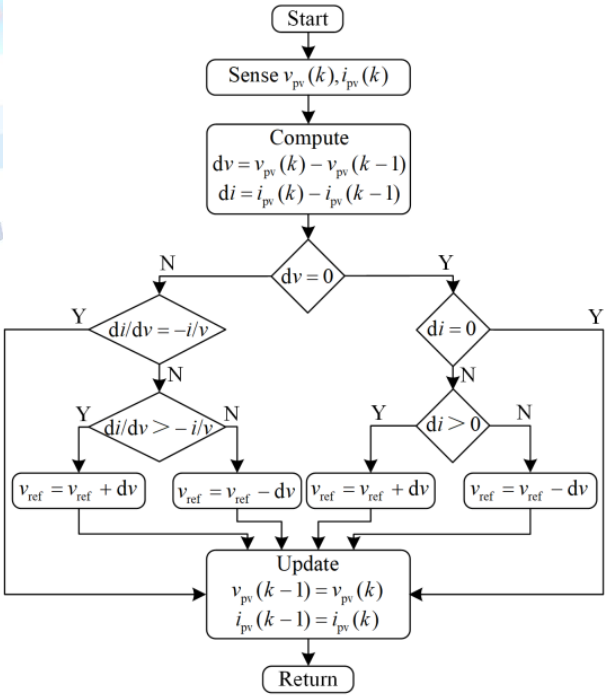

Fig. 4. Flow chat of modified incremental conductance maximum power point algorithm

B. Wind Energy System Configuration using PMSG

A wind turbine is mechanically connected to a PMSG (Permanent Magnet Synchronous Generator) in this setup. Directly delivered to the microgrid's DC bus or

rectified to DC via a Voltage Source Inverter (VSI) for AC load/grid interface, the PMSG's electrical output is variable-frequency AC.

1. Wind Turbine Power Output:

The mechanical power extracted from wind is given by:

$$P_{wind} = \frac{1}{2} \cdot \rho \cdot A \cdot v^3 \cdot C_P(\lambda, B) \quad (6)$$

Where: ρ = Air density (kg / m^3), $A = \pi R^2$ swept area of turbine blades, v = wind speed (m/s), C_P = power coefficient (function of tip speed ratio λ and pitch angle β)

2. Tip Speed Ratio λ:

$$\lambda = \frac{\omega_t R}{v} \quad (7)$$

Where: ω_t: Turbine angular speed (rad/s), R: Blade radius (m)

3. PMSG Modeling (dq-axis):

PMSG electrical dynamics in dq-frame:

$$V_d = R_s i_d + \frac{d\psi_d}{dt} - \omega_e \psi_q \quad (8)$$

$$V_q = R_s i_q + \frac{d\psi_q}{dt} - \omega_e \psi_d \quad (9)$$

$$T_e = \frac{3}{2} P\left(\psi_d i_q - \psi_q i_d\right) \quad (10)$$

Where: R_s: Stator resistance, ψ_d,ψ_q: d and q-axis flux linkages, ω_e : Electrical angular speed, T_e : Electromagnetic torque, P: Number of pole pairs

4. Control on the Machine Side

The creation of wind speed references is crucial for the machine-side control to maximize the wind turbine's power output. An active rectifier-connected PMSG's control circuit is illustrated in Figure 5. To calculate the reference rotor speed, the optimal ratio of the tip speed to the actual wind speed is utilized. The speed at which this is measured is:

$$\omega_m^{opt} = \frac{\lambda'_{opt} v_w}{R} \quad (11)$$

The speed of the reference rotor is represented by ω_m^{opt}. The PI speed controller is used to limit the speed error, which is calculated from the ideal wind speed and the actual speed of the PMSM, as reference electromagnetic torque. This means:

$$\omega_r^{error} = \omega_m^{opt} - \omega_r \quad (12)$$

$$T_e^* = k_{p,s}(\omega_r^{error}) + k_{i,s} \int (\omega_r^{error})\, dt \quad (13)$$

The variables ω_r^{error}, T_e^*, $k_{p,s}$, and$k_{i,s}$ denote the rotor speed error, reference electromagnetic torque, proportional gain, and integral gain, respectively, of the speed controller.

The reference q-axis current $\left(i_{qm}^*\right)$ is:

$$i_{qm}^* = \frac{4T_e^*}{3P} \quad (14)$$

An inner loop current controller regulates the machine side converter, which in turn generates the reference voltage. The coordinates on the d-q axis are:

$$v_{dm}^* = k_{p,mc}(i_{dm}^* - i_{ds}) + k_{i,mc} \int (i_{dm}^* - i_{ds})\, dt - \omega_e L_s i_{qs} \quad (15)$$

$$v_{qm}^* = k_{p,mc}\left(i_{qm}^* - i_{qs}\right) + k_{i,mc} \int \left(i_{qm}^* - i_{qs}\right) dt + \omega_e (L_s i_{ds} + \lambda_m) \quad (16)$$

The variables v_{dm}^* and v_{qm}^* on the d-q axis represent the reference machine voltage, i_{dm}^* and i_{qm}^* on the d-q axis represent the reference stator current, and the variables $k_{p,mc}$ and $k_{i,mc}$ represent the component gains of the machine current controller, respectively.

Using inverse park transformation, the voltage references on the d-q axis are transformed into three-phase machine voltage references, allowing the wind turbine to achieve its maximum output. The active rectifier on the machine side is operated by pulse width modulation (PWM) generators, which employ these three-phase machine voltage references.

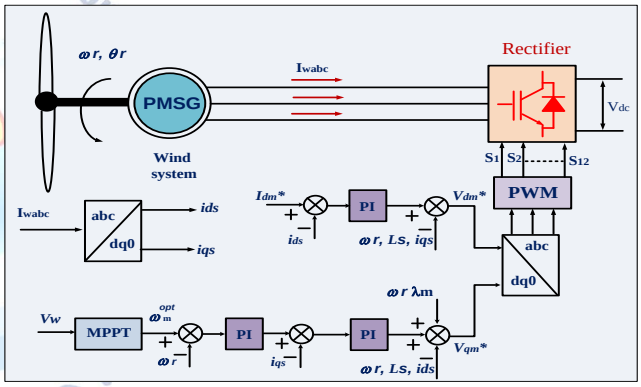

Fig.5 Wind conversion controller

C. Battery Energy Storage System (BESS) Configuration

Energy storage devices are essential for microgrids that use renewable power sources, such as wind turbines and solar PV, since they allow the system to maintain power during times of high demand or low output. It consists of a battery management system (BMS), a bidirectional DC-DC converter, and an array of batteries. The BESS switches between charging and discharging modes of operation in response to changes in the load and generation. Discharging involves maintaining the DC bus voltage by drawing power from the battery, as contrast to charging, which involves transferring power from the DC bus to the battery. The bidirectional converter regulates the voltage correctly by letting this energy flow in both directions. The power needs and permitted ripple limits determine the inductor and capacitor that the converter uses when operating in

Continuous Conduction Mode (CCM). Battery management systems (BMSs) keep the batteries running at peak efficiency by keeping tabs on their temperature, voltage, current, and state of charge (SOC). The solution enhances the microgrid's overall dependability and flexibility by contributing to the reduction of peak loads, improvement of power quality, and provision of backup power.

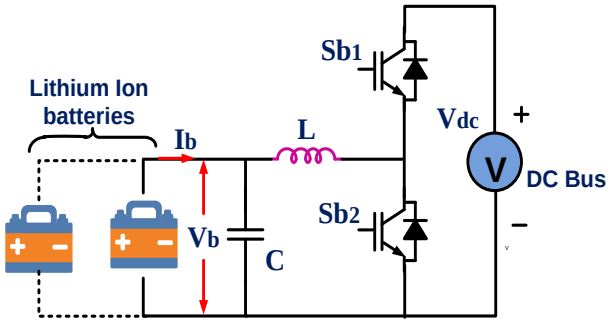

Fig.6 principle operation bidirectional dc-dc buck boost converter

1. Battery Terminal Voltage:

$$V_{bat} = V_{oc} - I_{bat} \cdot R_{bat} \quad (17)$$

2. State of Charge (SOC):

$$soc(t) = soc(0) - \frac{1}{C_{bat}} \int_0^t I_{bat}(t)\, dt \quad (18)$$

Where C_{bat} is the battery capacity in Ah.

3. Inductor Design for Bidirectional Converter (Buck/Boost):

$$L = \frac{V_{in} \cdot (1-D)}{f_s \cdot \Delta I_L} \quad (19)$$

Where V_{in}: input voltage, D: duty cycle, f_s: switching frequency, ΔI_L: inductor ripple current

4. Capacitor Design:

$$C = \frac{I_o \cdot D}{f_s \cdot \Delta V_o} \quad (20)$$

Where I_o: output current, ΔV_o: allowable output voltage ripple

D. Controller Designing for BESS

Battery Energy Storage Systems (BESS) frequently employ the double-loop control method to provide steady and precise regulation of the DC bus voltage and battery current, particularly during dynamic charging and discharging events. The technique is composed of an outside voltage control loop and an inner current control loop. It is the responsibility of the outer voltage loop to regulate the DC bus voltage V𝒹c by producing a reference current Iref for the inner loop. To keep the bus stable and maintain power balancing between sources and loads, it compares the recorded DC bus voltage with the reference voltage V𝒹c* and processes the error using a PI controller. Because of its increased speed, the inner current loop is able to change the duty cycle D of the converter to follow the reference current Iref. This improves the system's responsiveness and makes voltage swings less noticeable by charging or discharging the battery exactly according to system needs. As a result of their dependability and ease of implementation, PI controllers are usually used to implement both loops. A bidirectional DC-DC converter (typically a buck-boost or bidirectional interleaved converter) has its duty cycle modulated by the inner loop's output, guaranteeing steady performance in both charging and discharging modes.

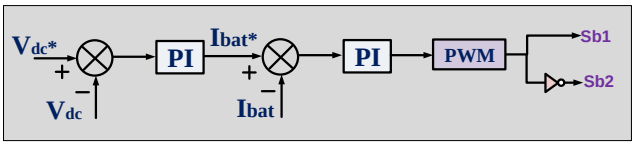

Fig. 7 double loop ev charging controller

1. Voltage Error Calculation:

$$e_v(t) = V_{dc}^* - V_{dc} \quad (21)$$

2. PI Voltage Controller Output (Reference Current):

$$I_{ref}(t) = K_{pv} \cdot e_v(t) + K_{iv} \int_0^t e_v(\tau) d\tau \quad (22)$$

3. Current Error Calculation:

$$e_i(t) = I_{ref}(t) - I_{bat}(t) \quad (23)$$

4. PI Current Controller Output (Duty Cycle Signal):

$$D(t) = k_{pi} \cdot e_i(t) + k_{ii} \int_0^t e_i(\tau) d\tau \quad (24)$$

E. AC Load Configuration using PMSM

The PMSM's exceptional torque-density and dynamic reactivity make it an ideal AC load for renewable-integrated energy systems and electric vehicles. To run the motor, the PMSM requires a three-phase Voltage Source Inverter (VSI), which takes the direct current (DC) output from renewable energy sources or energy storage systems and turns it into a sinusoidal alternating current (AC) supply. Using Field-Oriented Control (FOC) or Vector Control, the motor is usually controlled in the d-q rotating reference frame. This allows for decoupled control of flux and torque, much like in DC motors. A position sensor (usually an encoder), a speed controller, and two current controllers (d- and q-axis) make up the control system. In surface-mounted PMSMs, the maximum torque per ampere (MTPA) control is often achieved by setting the d-axis current id to zero, while the q-axis current iq directly controls the torque.

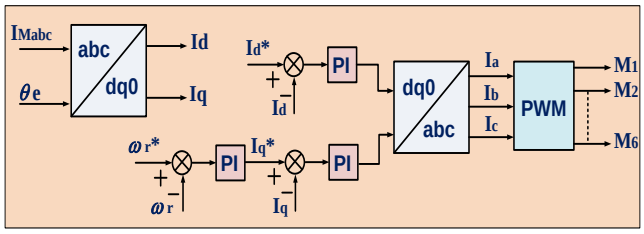

Fig. 8 controller design of AC load PMSM water pump system

1. Speed Error Calculation

Use the speed reference ω_r^* and actual rotor speed ω_r:

$$e_\omega = \omega_r^* - \omega_r \quad (25)$$

2. Torque Command from PI Speed Controller

Using the PI controller for speed control:

$$T_e^* = k_P(\omega_r^* - \omega_r) + k_i \int (\omega_r^* - \omega_r)dt \quad (26)$$

Where: T_e^* = reference electromagnetic torque, k_P, k_i= proportional and integral gains

3. q-Axis Current Reference i_q^*

For a surface-mounted PMSM (no saliency), torque is proportional to i_q:

$$i_q^* = \frac{2}{3} \cdot \frac{T_e^*}{P \cdot \lambda_m} \quad (27)$$

Where: P = number of pole pairs, λ_m = permanent magnet flux linkage

4. Set d-Axis Current Reference i_d^* to 0

For maximum efficiency:

$$i_d^* = 0 \quad (28)$$

5. Current Errors (d-q axes)

$$e_d = i_d^* - i_d \quad (29)$$

$$e_q = i_q^* - i_q \quad (30)$$

6. Voltage Reference Generation via PI Controllers

d-axis voltage:

$$v_d^* = k_{pd} e_d + k_{id} \int e_d \, dt - \omega_e L_q i_q \quad (31)$$

q-axis voltage:

$$v_q^* = k_{pq} e_q + k_{iq} \int e_q \, dt - \omega_e L_d i_d \quad (32)$$

Where: L_d, L_q = d and q-axis inductances, $\omega_e = P \cdot \omega$ = electrical angular speed

7. Inverse Park Transformation

Transform v_d^*, v_q^* to stationary αβ frame:

$$\begin{bmatrix} v_\alpha \\ v_B \end{bmatrix} = \begin{bmatrix} \cos\theta & -\sin\theta \\ \sin\theta & \cos\theta \end{bmatrix} \begin{bmatrix} v_d^* \\ v_q^* \end{bmatrix} \quad (33)$$

8. Inverse Clarke Transformation

Convert αβ voltages to 3-phase (abc):

$$\begin{bmatrix} v_a \\ v_b \\ v_c \end{bmatrix} = \begin{bmatrix} 1 & 0 \\ -1/2 & \sqrt{3}/2 \\ -1/2 & -\sqrt{3}/2 \end{bmatrix} \begin{bmatrix} v_\alpha \\ v_\beta \end{bmatrix} \quad (34)$$

The V_{abc} values are compared with a carrier signal (triangular wave) to generate gate signals for the inverter switches driving the PMSM.

4. Grid Side Converter Controller

The rapid growth of distributed energy resources like solar photovoltaic systems and wind power has led to the development of advanced microgrid architectures. However, these renewable sources pose challenges in maintaining voltage stability, power quality, and real-time load balancing when operating alongside conventional utility grids. To address these concerns, a hybrid AC/DC microgrid is proposed that integrates solar photovoltaic panels, wind-driven permanent magnet synchronous generators, and a battery energy storage system through a common DC-link. This configuration reduces energy conversion losses and increases overall system efficiency. The design uses a Distributed Power Flow Controller (DPFC) to control active and reactive power, mitigating voltage sags, swells, and current harmonics. Its unique architecture allows independent and flexible operation without bulky DC links, resulting in enhanced power quality and better voltage regulation across both AC and DC subsystems. The inclusion of a battery energy storage system strengthens the microgrid's performance by supporting peak load conditions, providing backup power during outages, and stabilizing DC-link voltage during transient events. The grid-side converter plays a key role in interfacing the hybrid microgrid with the utility grid, converting DC-link voltage into synchronized three-phase AC voltage for power exchange with the grid. A double-loop control strategy regulates voltage and current, ensuring smooth operation even under fluctuating load and generation conditions. The proposed microgrid supports seamless operation under both grid-connected and islanded conditions, with an intelligent energy management strategy ensuring proper distribution of AC and DC loads according to available renewable power and load demands. The hybrid structure supports both linear and nonlinear loads, and the DPFC significantly improves power quality by reducing total harmonic distortion and stabilizing voltage profiles.

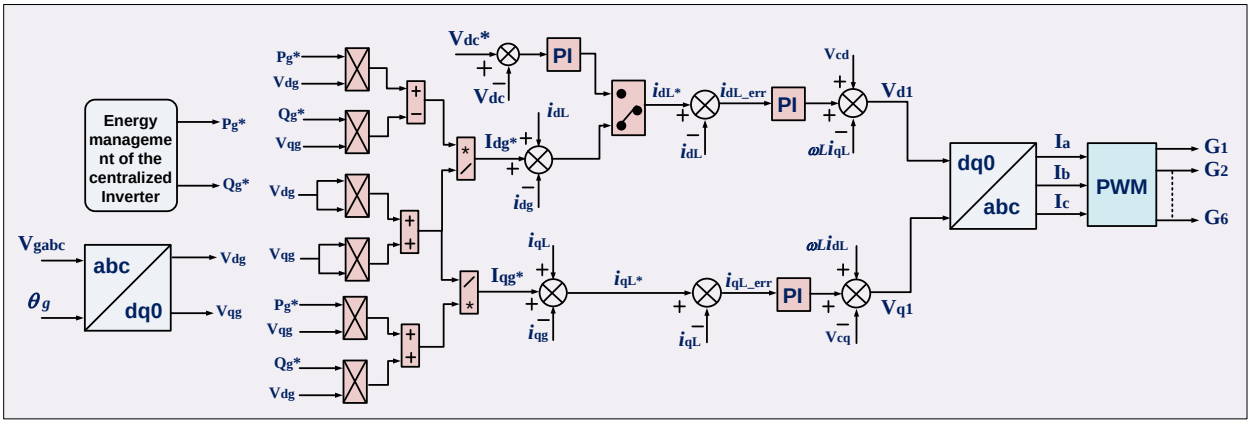

Fig. 9. Control diagram of the centralized inverter connected with utility grid.

The available real power from the renewable energy source is:

$$P_{gen} = P_{wind} + P_{solar} + P_{battery} \quad (35)$$

Where $P_{wind}, P_{solar}, P_{battery}$ represent power generated by wind, solar and power stored in battery.

The power used by the local load P_{local} is:

$$P_{local} = P_{dc(dc\ load)} + P_{ac(pump\ load)} \quad (35)$$

Where $P_{dc(dc\ load)}$ and $P_{ac(pump\ load)}$ represent DC load and pump load.

The reference active power injection through the centralized inverter is:

$$P_g^* = P_{gen} - P_{local} \quad (36)$$

Where P_g^* represents reference active power.

The *d-q* axis grid current references are:

$$i_{dg}^* = \frac{v_{dg}P_g^* - v_{qg}Q_g^*}{v_{dg}^2 + v_{qg}^2} \quad (37)$$

$$i_{qg}^* = \frac{v_{qg}P_g^* - v_{dg}Q_g^*}{v_{dg}^2 + v_{qg}^2} \quad (38)$$

The variables i_{dg}^* and i_{qg}^* stand for the reference grid current and reactive and active power, respectively, on the d-q axis. The variables v_{dg} and v_{qg}, on the other hand, indicate the grid voltage on the same d-q axis.

For optimal real power transfer to the grid, the inductor currents along the reference d-q axis must be maximized. The d-q axis reference inductor currents are supplied by the following formula, which is derived from the real grid currents, actual inductor currents, and instantaneous d-q axis references:

$$i_{dL}^* = i_{dg}^* + i_{cd} = i_{dg}^* + (i_{dL} - i_{dg}) \quad (39)$$

$$i_{qL}^* = i_{qg}^* + i_{cd} = i_{qg}^* + (i_{qL} - i_{qg}) \quad (40)$$

Where i_{dL}^*, i_{qL}^* denote the reference inductor current on the d-q axis, i_{dg}^*, i_{qg}^* the grid current on the d-q axis, i_{dL}, i_{qL} the filter inductor current on the d-q axis, and i_{cd}, i_{cd} the filter capacitor current on the d-q axis may be found.

The reference voltages for grid-side control are generated by the inner loop current controller, which manages inductor current errors. To keep the centralized inverter running reliably and steadily, they are used as:

$$v_{dL}^* = k_{p,gc}(i_{dL}^* - \dot{i}_{dL}) + k_{i,gc}\int (i_{dL}^* - i_{dL})dt - \omega L_s i_{qL} + v_{cd} \quad (41)$$

$$v_{qL}^* = k_{p,gc}(i_{qL}^* - \dot{i}_{qL}) + k_{i,gc}\int (i_{qL}^* - i_{qL})dt - \omega L_s i_{dL} + v_{cq} \quad (42)$$

Here, v_{dL}^*, and v_{qL}^* stand for the reference inductive voltage on the d-q axis, $k_{p,gc}$ for the proportional gain of the grid current controller, and $k_{i,gc}$ for the integral gain of the same controller.

In order to provide switching signals for the three-phase grid-connected inverter, the inductive voltage references on the d-q axis are transformed into three-phase voltage references using inverse park transformation and then inputted into the PWM generator.

5. Control of DPFC

The DPFC-PV-WE-ESS system integrates renewable energy sources with advanced power quality monitoring and compensation methods. By mitigating voltage-related disturbances such as sags, swells, harmonics, and flickers, the system enhances grid reliability and operational efficiency. Utilizing the distributed nature of the DPFC, which includes both series and shunt converters operating independently, this architecture, optimizes control flexibility and effectiveness. The shunt converter addresses power quality issues such as reactive power compensation and suppression of load current harmonics by dynamically adjusting the injection of compensating currents. This capability supports the smooth integration of renewable

sources, including photovoltaic panels for solar energy harvesting and wind turbines that convert wind energy into electrical power. To shield sensitive loads from poor-quality grid voltage, the series converter injects controlled voltages in synchronization with the grid waveform, effectively compensating for voltage fluctuations and imbalances. The integration of an energy storage system enhances grid support by supplying backup power during outages and regulating power flow under dynamic load or generation conditions. The DPFC-PV-WE-ESS system maintains the DC-link voltage at a predefined reference level using a proportional-integral (PI) controller. It utilizes the Synchronous Reference Frame (SRF) method to manage current distortion and maintain voltage stability. For accurate synchronization with the grid, the system employs phase-locked loop (PLL) data to transform load currents into the d–q–0 reference frame. A moving average filter (MAF) is applied to ensure smooth control action with minimal transient disturbances. Overall, the DPFC-PV-WE-ESS configuration provides a robust solution to power quality challenges, enables seamless integration of distributed renewable energy sources, and contributes to building a more sustainable and resilient power system.

A. Control of Shunt Compensator

Phase voltages are calculated by dividing line voltage by the square root of three, which accurately determines the voltage supplied to each phase in a three-phase power system. This method accounts for the phase shift between line and phase voltages, ensuring efficient operation for each phase.

$$V_a = \frac{1}{3}(2V_{ab} + V_{bc}) \quad (17)$$

$$V_b = \frac{1}{3}(-V_{ab} + V_{bc}) \quad (18)$$

$$V_c = \frac{1}{3}(-V_{ab} - 2V_{bc}) \quad (19)$$

The terminal voltage Vt is derived from phase voltages as,

$$V_t = \sqrt{(2(V_a^2 + V_b^2 + V_c^2)/3)} \quad (20)$$

DC Loss Component Estimation

The sensed DC link voltage (V_{dc}) is compared with the DC link reference voltage ($V_{dc\,ref}$) and the difference in voltage (V_{dce}) is acquired.

$$V_{dce}(n) = V_{dcref}(n) - V_{dc}(n) \quad (21)$$

The error is fed to the DC link voltage controller for minimization. The controller is governed as,

$$w_{loss}(n) = w_{loss}(n-1) + k_{il}\{V_{dc\,e}(n) - V_{dce}(n-1)\} + k_{Pl}\{V_{dce}(n)\} \quad (22)$$

Where, k_{il} and k_{Pl} are the controller gains.

Estimation of Feed-Forward Components of RERs

Making use of the feed-forward terms linked to the RERs improves the dynamic responsiveness. To determine the RER feed-forward terms, one must do the following:

$$I_{PVg} = \frac{2P_{PV}}{3V_t} \quad (23)$$

$$I_{wind} = \frac{2P_{\text{wind}}}{3V_t} \quad (24)$$

Where P_{PV} and I_{PVg} represent PV power and its feed-forward term, P_{wind} and I_{wind} stand for wind power and its feed-forward term, respectively.

$$MAF(s) = \frac{1-e^{-T_w s}}{T_w s} \quad (25)$$

Eliminating harmonics from the current element on the d-axis is a crucial function of the Moving Average Filter (MAF). By adjusting its window length to half of the fundamental time period, we may remove harmonics without affecting the fundamental frequency component. The component of fundamental frequency stays the same due to its DC gain of one. To get rid of higher-order harmonics, however, we dampen integer multiples of the window depth. Maximizing the power extraction from the PV array and wind output, as well as improving power quality and performance, are all dependent on a control system that has been carefully built and tuned. An important part of this system is the equivalent current component that is generated by the wind and PV array.

$$I_{sd}^{*} = I_{L\,df} + I_{loss} - I_{Pvg} - I_{wg} \quad (26)$$

The currents in the abc domain reference grid are transformed from I_{sd}^{*}. In order to provide the gating pulses for the shunt converter, a hysteresis current controller compares the reference grid currents with the measured grid currents.

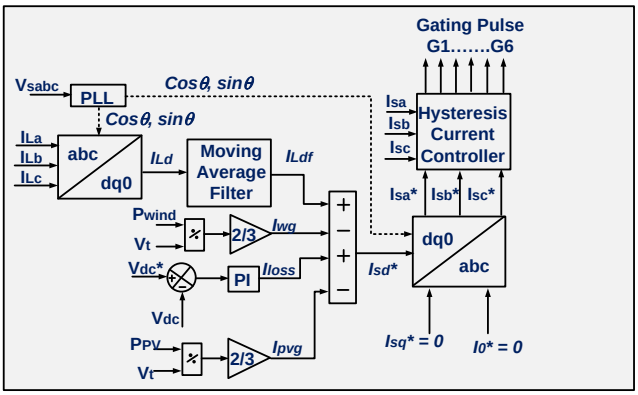

Fig. 10 Control Structure of Shunt Compensator

B. Designing for series converter controller

The series converter is designed to enhance power quality in grid-connected systems by mitigating voltage disturbances such as sags, swells, and harmonics. As a key component of the Dynamic Voltage Restorer (DVR), the series converter operates by injecting compensating voltage into the grid to maintain a stable power supply for critical loads as shown in fig.11. The series converter adjusts its operation based on real-time voltage fluctuations at the Point of Common Coupling (PCC). It continuously measures the grid voltage and injects the required compensating voltage using a predefined reference-based method. The system operates by directly sensing voltage variations and using pulse width modulation (PWM) techniques to regulate the injected voltage. The injected voltage is derived from real-time grid conditions, ensuring that voltage sags and swells are automatically corrected. To minimize harmonic distortion and maintain a sinusoidal voltage waveform, the series converter incorporates passive filtering techniques such as LC filters or transformer-based isolation to smooth the injected voltage. As solar power generation varies, the series converter dynamically adjusts the compensating voltage based on the available power from the photovoltaic (PV) system. This ensures that the load receives a constant and stable voltage supply, regardless of fluctuations in the grid. By eliminating the need for complex control mechanisms, the proposed system simplifies operation while still achieving effective voltage regulation and harmonic suppression, ensuring high power quality in renewable energy-integrated grid systems.

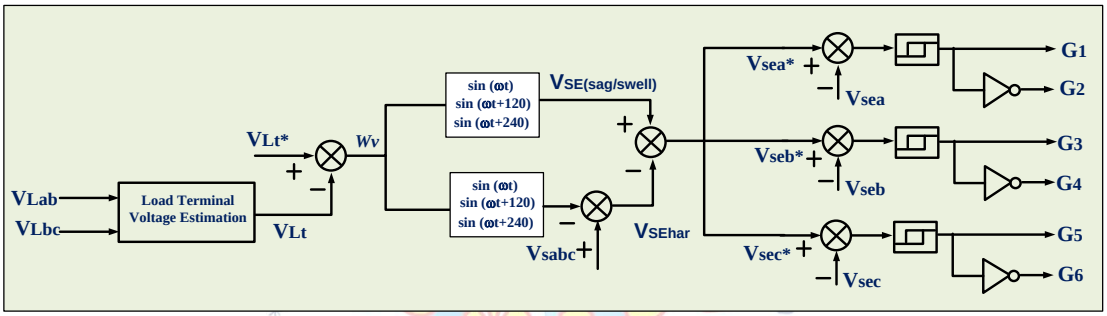

Fig.12 Series converter controller

6. Results and Discussion

A. Coordinated Control of Renewable Sources and Load Balancing in Microgrid Operation

Stable operation and improved power quality were achieved in the hybrid DC/AC microgrid system by coordinating renewable energy sources, a battery energy storage system (BESS), and a Distributed Power Flow Controller (DPFC). The microgrid generated 15.2 kW of renewable energy, with 8.5 kW from a wind-driven PMSG and 4.5 kW from a PV array under typical irradiance circumstances. The 2.2 kW battery system kept power balance during transient occurrences. A total of 37.53 kW was required, including 7.25 kW of DC loads, a 2.2 kW PMSM-based AC motor load, 25 kW of AC linear loads, and 3.08 kW of non-linear loads. A voltage source converter (VSC) connected the DC and AC microgrids for bidirectional power flow and DC bus stability at 380 V. A considerable fall in renewable generation occurred between 0.3 seconds and 1 second of operation due to a drop in wind speed from 13 to 8 m/s and a decrease in sun irradiation from 1000 to 750 W/m². Thus, wind and solar power outputs dropped from 13 kW to 7.5 kW. The battery system discharged at its full 2.2 kW rating to make up for the shortfall, while the grid dynamically balanced the power demand with renewable sources to meet the rest. Since the PMSM water pump load rose from zero to its maximal operational speed of 157 rad/s between 0.65 seconds and 1 second, the AC load likewise climbed to 2.2 kW. The suggested control technique maintained continuous and balanced power supply to all loads without microgrid instability despite dynamic situations and varying load and generation levels. The hierarchical control system dynamically regulated DC bus voltage and managed energy flow between renewable sources, the BESS, and the grid to prevent battery overcharging and power supply mismatches. The DPFC's series and shunt converters helped preserve system power quality. It mitigated grid disturbance-induced voltage sags and swells and lowered 3.08 kW non-linear load current harmonics. DPFC-free grid current has 7.3% total harmonic distortion (THD). DPFC decreased THD to <

3.1%, meeting IEEE-519 requirements. The DPFC enhanced voltage profiles at the point of common coupling (PCC), minimizing variances to ±2% and eliminating sensitive load performance loss. The device optimized grid-microgrid power flow, improving system dependability and power quality. MATLAB/Simulink simulations showed improved transient responsiveness, oscillation reduction, and system voltage and current stability. Even in changing weather, PV and wind MPPT algorithms maximized energy harvest. The battery's reaction during low generation prevented system collapse, while the DPFC's power quality management ensured clean, balanced supply to linear and non-linear AC loads. A complicated hybrid AC/DC microgrid operated smoothly, had better power quality, and delivered reliable power using the suggested control and coordination technique.

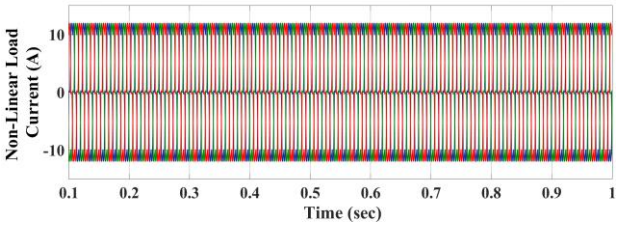

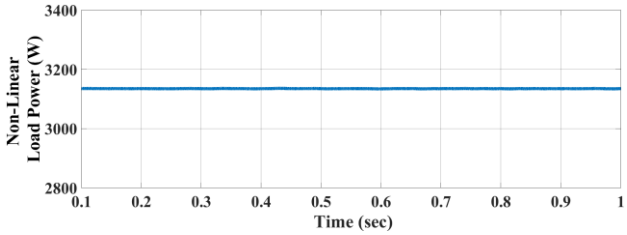

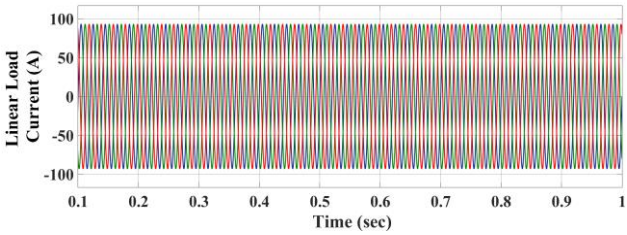

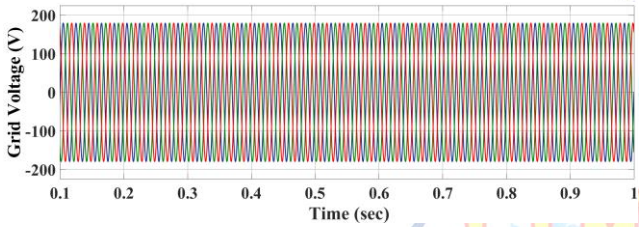

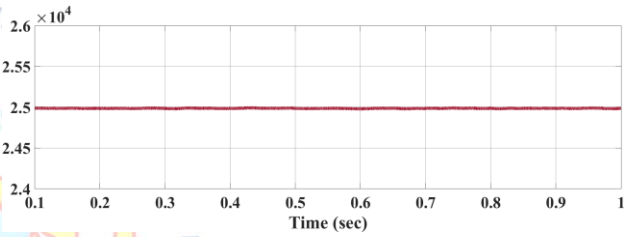

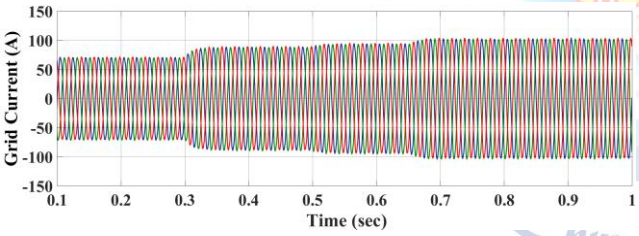

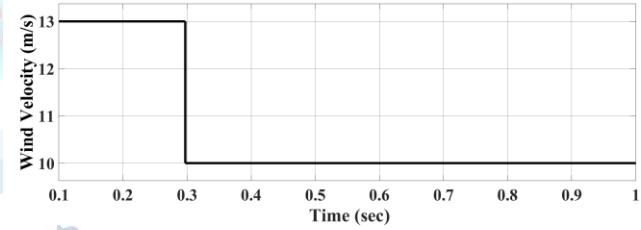

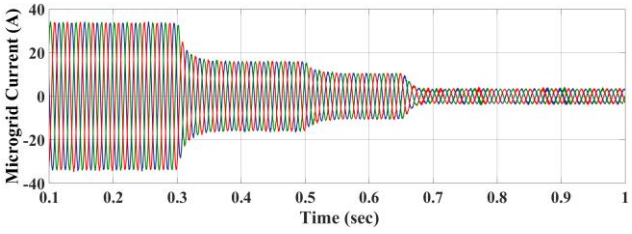

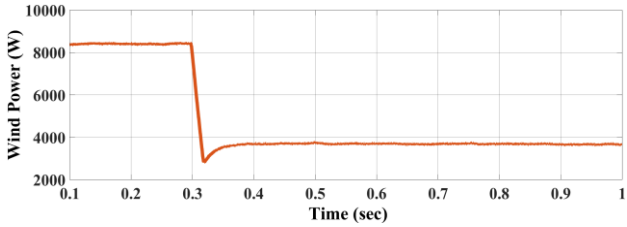

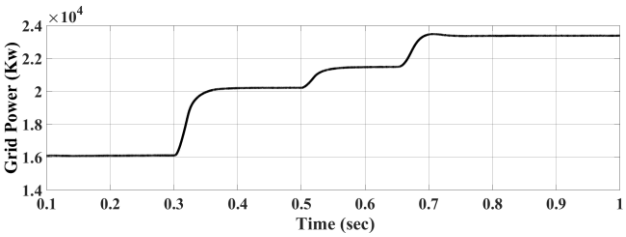

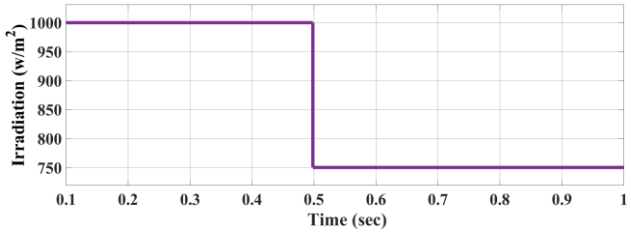

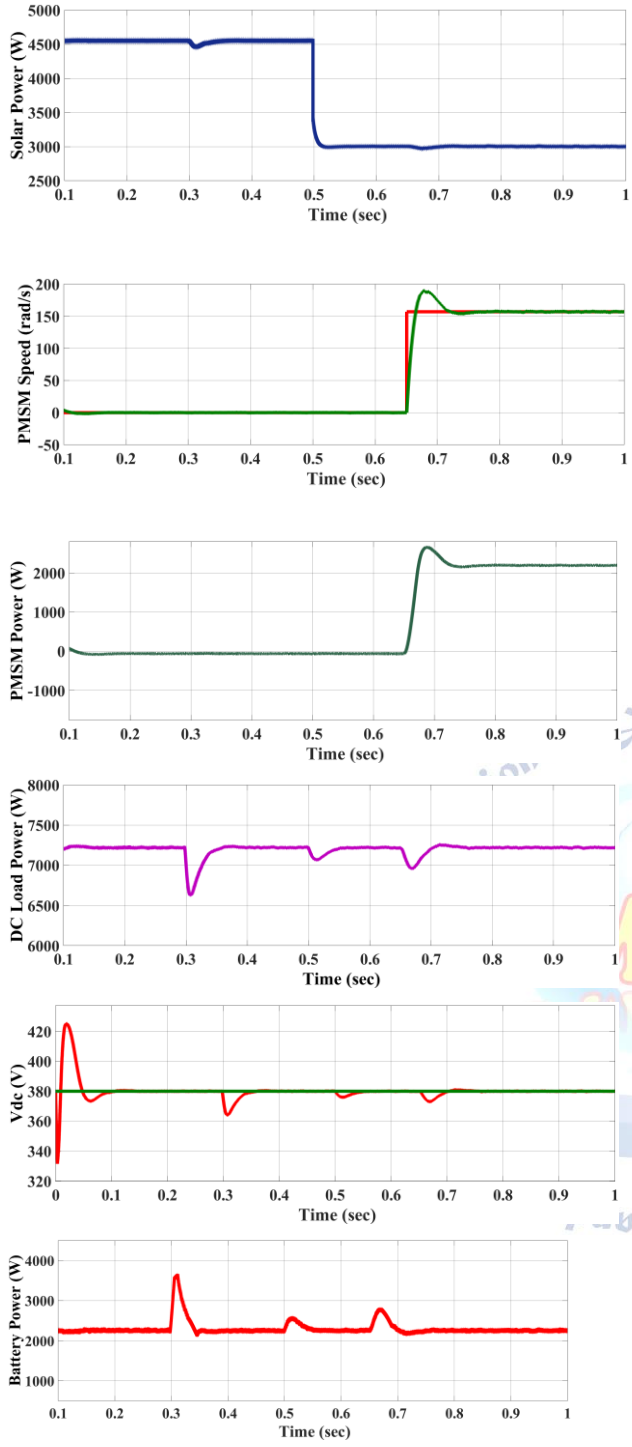

Fig.13 simulation results of Dynamic Power Coordination under Varying Generation and Load Conditions

B. DPFC-Based Voltage Sag and Swell Compensation

The simulation results validate the effectiveness of the Distributed Power Flow Controller (DPFC) in mitigating voltage disturbances such as sag and swell conditions, thereby significantly enhancing the power quality of the load supply, as illustrated in Fig. 16. Voltage sag is observed between 0.2 seconds and 0.4 seconds, attributed to a sudden increase in load demand or a temporary fault within the system. During this interval, the DPFC promptly injects the required compensating voltage through its series converter to restore the grid voltage to nominal levels, ensuring stable and uninterrupted power delivery to the connected linear and nonlinear loads. Subsequently, a voltage swell occurs between 0.6 seconds and 0.8 seconds, primarily due to a sudden drop in load demand or an unexpected surge in power generation from the integrated renewable sources. The DPFC efficiently absorbs the excess voltage using its shunt converter, thereby stabilizing the supply and preventing overvoltage conditions that could compromise sensitive equipment. Throughout the entire simulation period, the DPFC maintains a well-regulated and balanced voltage profile at the point of common coupling (PCC), minimizing voltage fluctuations. This consistent performance underscores the DPFC's role in ensuring a reliable and high-quality power supply within the hybrid AC/DC microgrid under dynamic operating conditions.

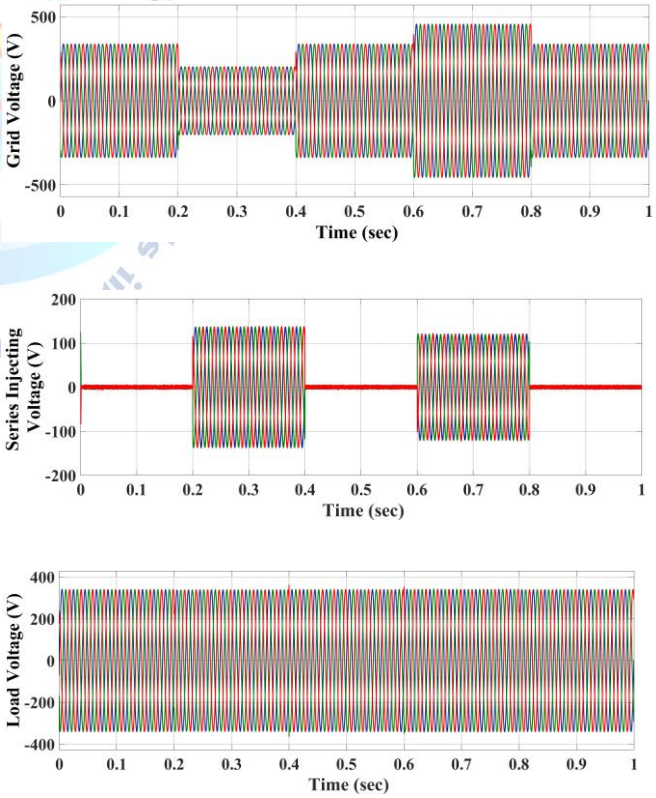

Fig. 14 Simulation results for sag and swell condition

The simulation results demonstrate a clear improvement in power quality with the implementation of the Distributed Power Flow Controller (DPFC). The grid current Total Harmonic Distortion (THD) with the

DPFC active is measured at approximately 3.09%, indicating effective harmonic mitigation and a more sinusoidal current waveform (Fig. 15a). Without the DPFC, the grid current THD rises to about 4.37%, showing increased harmonic distortion and poorer power quality due to the unmitigated effects of nonlinear loads and voltage disturbances (Fig. 15b). The non-linear load current THD is significantly higher at 23.03%, reflecting the substantial harmonic content generated by nonlinear loads connected to the system (Fig. 15c). These results confirm that the DPFC plays a vital role in reducing harmonics, improving voltage stability, and enhancing overall power quality within the hybrid AC/DC microgrid.

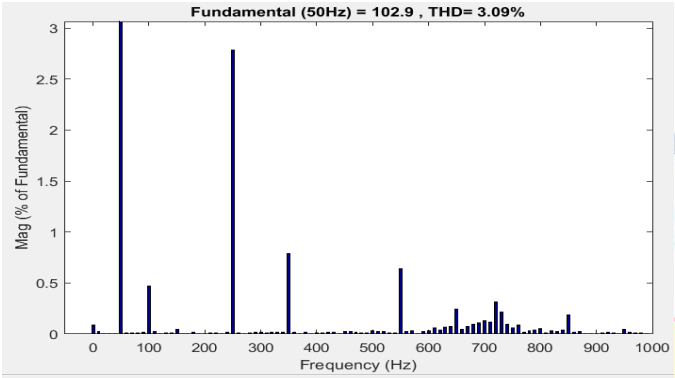

(a)

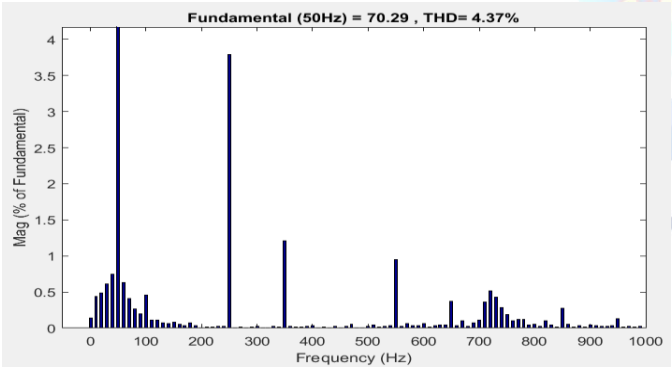

(b)

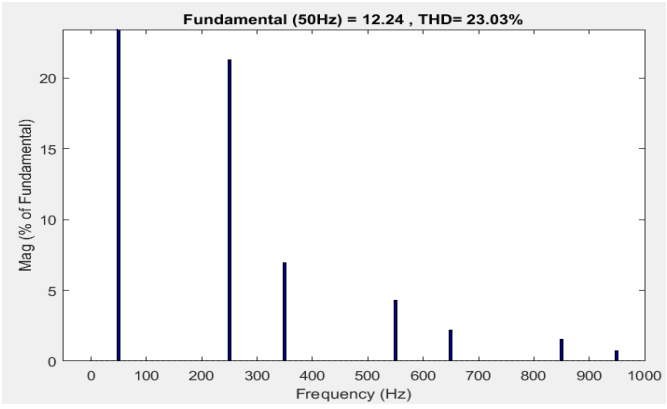

(c)

Fig, 15 (a) grid current THD with DPFC, (b) grid current THD without DPFC, (c) load current THD

7. Conclusion

This paper presents a comprehensive control strategy for a hybrid DC/AC microgrid that integrates photovoltaic (PV), wind energy, and a battery energy storage system (BESS) with a Distributed Power Flow Controller (DPFC) to improve system stability and power quality. By effectively coordinating renewable energy resources and storage systems through maximum power point tracking (MPPT) and bidirectional converters, the proposed system ensures continuous, reliable power supply under varying generation and load conditions. The incorporation of AC linear and non-linear loads and the implementation of a voltage source converter (VSC) at the grid interface further enhance the flexibility and performance of the microgrid. The DPFC, consisting of series and shunt converters, significantly mitigates voltage sags, swells, and current harmonics, leading to a notable reduction in Total Harmonic Distortion (THD) and an overall improvement in voltage and current profiles. Simulation results in MATLAB/Simulink validate the effectiveness of the proposed system in maintaining stable operation, achieving superior transient response, and ensuring power quality compliance under dynamic grid and load disturbances. The coordinated control and energy management strategy enable reliable bidirectional power flow and contribute to the development of efficient, sustainable, and resilient future power systems.

Conflict of interest statement

Authors declare that they do not have any conflict of interest.

REFERENCES

[1] K. Padmanathan, U. Govindarajan, V. K. Ramachandaramurthy, A. Rajagopalan, N. Pachaivannan, U. Sowmmiya, S. Padmanaban, J. B. Holm-Nielsen, S. Xavier, and S. K. Periasamy, ``A sociocultural study on solar photovoltaic energy system in India: Strati_cation and policy implication,'' J. Cleaner Prod., vol. 216, pp. 461_481, Apr. 2019.

[2] R. M. Elavarasan, G. Sha_ullah, S. Padmanaban, N. M. Kumar, A. Annam, A. M. Vetrichelvan, L. Mihet-Popa, and J. B. Holm-Nielsen, ``A comprehensive review on renewable energy development, challenges, and policies of leading Indian states with an international perspective,'' IEEE Access, vol. 8, pp. 74432_74457, 2020.

[3] S. Kumar, R. K. Saket, D. K. Dheer, J. B. Holm-Nielsen, and P. Sanjeevikumar, ``Reliability enhancement of electrical power system including impacts of renewable energy sources: A

comprehensive review," IET Gener., Transmiss. Distrib., vol. 14, no. 10, pp. 1799_1815, May 2020.

[4] I. Masenge and F. Mwasilu, ``Hybrid solar PV-wind generation system coordination control and optimization of battery energy storage system for rural electrification," in Proc. IEEE PES/IAS PowerAfrica, Aug. 2020, pp. 1_5.

[5] N. Priyadarshi, S. Padmanaban, M. S. Bhaskar, F. Blaabjerg, and J. B. Holm-Nielsen, ``An improved hybrid PV-wind power system with MPPT for water pumping applications," Int. Trans. Electr. Energy Syst., vol. 30, no. 2, p. e12210, Feb. 2020.

[6] S. Padmanaban, K. Nithiyananthan, S. P. Karthikeyan, and J. B. Holm-Nielsen, Microgrids. Boca Raton, FL, USA: CRC Press, 2020.

[7] A. Suman, ``Role of renewable energy technologies in climate change adaptation and mitigation: A brief review from Nepal," Renew. Sustain. Energy Rev., vol. 151, Nov. 2021.

[8] L. Varshney, A. S. S. Vardhan, S. Kumar, R. Saket, and P. Sanjeevikumar, ``Performance characteristics and reliability assessment of self-excited induction generator for wind power generation," IET, Renew. Power Gener., vol. 15, pp. 1927_1942, 2021.

[9] M. Seapan, Y. Hishikawa, M. Yoshita, and K. Okajima, ``Temperature and irradiance dependences of the current and voltage at maxi- mum power of crystalline silicon PV devices," Sol. Energy, vol. 204, pp. 459_465, Jul. 2020.

[10] F. Mebrahtu, B. Khan, P. Sanjeevikumar, P. K. Maroti, Z. Leonowicz, O. P. Mahela, and H. H. Alhelou, ``Harmonics mitigation in industrial sector by using space vector PWM and shunt active power _lter," in Proc. IEEE Int. Conf. Environ. Electr. Eng., IEEE Ind. Commercial Power Syst. Eur. (EEEIC/I&CPS Europe), Jun. 2020, pp. 1_6.

[11] S. Vadi, S. Padmanaban, R. Bayindir, F. Blaabjerg, and L. Mihet Popa, ``A review on optimization and control methods used to provide transient stability in microgrids," Energies, vol. 12, no. 18, p. 3582, Sep. 2019.

[12] N. Priyadarshi, S. Padmanaban, R. K. Ghadai, A. R. Panda, and R. Patel, ``Advances in power systems and energy management select proceed- ings of ETAEERE 2020," in Power System and Energy. Springer, 2020, p. 4.

[13] E. Sundaram and M. Venugopal, ``On design and implementation of three phase three level shunt active power _lter for harmonic reduction using synchronous reference frame theory," Int. J. Electr. Power Energy Syst., vol. 81, pp. 40_47, Oct. 2016.

[14] A. Raj, S. R. Arya, and J. Gupta, ``Solar PV array-based DC_DC converter with MPPT for low power applications," Renew. Energy Focus, vol. 34, pp. 109_119, Sep. 2020.

[15] C. H. Basha and C. Rani, ``Different conventional and soft computing MPPT techniques for solar PV systems with high step-up boost con- verters: A comprehensive analysis," Energies, vol. 13, no. 2, p. 371, Jan. 2020.

[16] J. D. Kumar, K. Mantosh, M. S. Bhaskar, P. Sanjeevikumar, J. B. H. Nielsen, and Z. Leonowicz, ``Investigation studies of DC-DC boost converter with proportional-integral-derivative controller using optimization techniques," in Proc. IEEE Int. Conf. Environ. Electr. Eng., IEEE Ind. Commercial Power Syst. Eur. (EEEIC/I&CPS Europe), Jun. 2020, pp. 1_5.

[17] K. Gulyamov, R. Yunusov, S. Dovudov, B. Sharifov, A. Ghulomzoda, and M. Safaraliev, ``Increase in power of DC/DC converters with increased number of conversion channels," in Proc. Ural Smart Energy Conf. (USEC), Nov. 2020, pp. 59_62.

[18] N. Hawkins, B. Bhagwat, and M. L. McIntyre, ``Nonlinear current-mode control of SCIG wind turbines," Energies, vol. 14, no. 1, p. 55, Dec. 2020.

[19] A. M. M. dos Santos, L. T. P. Medeiros, L. P. S. Silva, I. D. S. Junior, V. S. de C. Teixeira, and A. B. Moreira, ``Wind power system connected to the grid from squirrel cage induction generator (SCIG)," in Proc. IEEE 15th Brazilian Power Electron. Conf., 5th IEEE Southern Power Electron. Conf. (COBEP/SPEC), Dec. 2019, pp. 1_6.

[20] A. K. S. Tomar, K. K. Gautam, and A. Lodhi, ``Integration of SCIG wind energy conversion systems to the grid," Int. J. Eng. Sci. Invention, vol. 9, no. 6, pp. 28_36, 2020.

[21] B. B. Adetokun, C. M. Muriithi, and J. O. Ojo, ``Voltage stability analysis and improvement of power system with increased SCIG-based wind system integration," in Proc. IEEE PES/IAS PowerAfrica, Aug. 2020, pp. 1_5.

[22] M. Xu, L. Wu, H. Liu, and X. Wang, ``Multi-objective optimal scheduling strategy for wind power, PV and pumped storage plant in VSC-HVDC grid," J. Eng., vol. 2019, no. 16, pp. 3017_3021, Mar. 2019.

[23] P. Manoharan, U. Subramaniam, T. S. Babu, S. Padmanaban, J. B. Holm-Nielsen, M. Mitolo, and S. Ravichandran, ``Improved perturb and observation maximum power point tracking technique for solar photovoltaic power generation systems," IEEE Syst. J., vol. 15, no. 2, pp. 3024_3035, Jun. 2021.

[24] M. H. Reza and M. A. Shobug, ``Ef_ciency evaluation of P&O MPPT technique used for maximum power extraction from solar pho- tovoltaic system," in Proc. IEEE Region Symp. (TENSYMP), Jun. 2020, pp. 1808_1811.

[25] A. Ali, K. Almutairi, S. Padmanaban, V. Tirth, and S. Algarni, ``Investigation of MPPT techniques under uniform and non-uniform solar irradiation condition_A retrospection," IEEE Access, vol. 8, pp. 127368_127392, 2020.

[26] G. S. Chawda, A. G. Shaik, O. P. Mahela, S. Padmanaban, and J. B. Holm-Nielsen, ``Comprehensive review of distributed facts control algorithms for power quality enhancement in utility grid with renewable energy penetration," IEEE Access, vol. 8, pp. 107614_107634, 2020.

[27] A. Sen, A. Banerjee, and H. Nannam, ``A comparative analysis between two DPFC models in a grid connected hybrid solar-wind generation system," in Proc. IEEE Int. Conf. Power Electron., Smart Grid Renew. Energy (PESGRE), Jan. 2020, pp. 1_6.

[28] X. Zhai, A. Tang, X. Zou, X. Zheng, and Q. Xu, ``Research on DPFC capacity and parameter design method," in Proc. IEEE Int. Conf. Inf. Technol., Big Data Artif. Intell. (ICIBA), vol. 1, Nov. 2020, pp. 978_982.

[29] J. H.Woo, L.Wu, S. M. Lee, J.-B. Park, and J. H. Roh, ``D-STATCOM d-q axis current reference control applying DDPG algorithm in the distribution system," IEEE Access, vol. 9, pp. 145840_145851, 2021.

[30] G. Balasubramani, V. Thangavelu, M. Chinnusamy, U. Subramaniam, S. Padmanaban, and L. Mihet-Popa, ``Infrared thermography based defects testing of solar photovoltaic panel with fuzzy rule-based evaluation," Energies, vol. 13, no. 6, p. 1343, Mar. 2020.